Pulsed laser crystallization of silicon–germanium films

T. Sameshima[a],*, H. Watakabe[a], H. Kanno[b], T. Sadoh[b], M. Miyao[b]

[a]Tokyo University of Agriculture and Technology, Koganei, Tokyo 184-8588, Japan
[b]Kyushu University, Fukuoka 812-8581, Japan

Abstract

Pulsed-XeCl excimer laser crystallization of germanium (Ge) and silicon–germanium (SiGe) alloy films formed on quartz glass substrates was investigated. The transient conductance measurements reveled that germanium films were rapidly melted and solidified because of low latent heat compared to silicon films. Formation of silicon–germanium alloy was also observed in the case of laser annealing the Ge/Si layered structure. The crystalline volume ratio was estimated almost 1.0 for $Si_{0.4}Ge_{0.6}$ films because of small disordered electronic states at grain boundaries, while it was 0.85 for Si films.
© 2005 Elsevier B.V. All rights reserved.

Keywords: Laser annealing; SiGe; Transient conductance measurement; Melt depth; Melt duration; Grain boundary

1. Introduction

Germanium and silicon–germanium (SiGe) have been attractive materials for transistor application because they can have a high carrier mobility especially in the tensile stressed case [1–3]. Pulsed laser induced crystallization of silicon films has been precisely investigated and widely applied to fabrication of polycrystalline silicon thin film transistors (poly-Si TFTs) [4–10]. The electrical and structural properties of polycrystalline silicon (poly-Si) thin films formed by pulsed laser irradiation have been reported. It has been also reported that tensile stressed poly-Si films are formed by laser crystallization on glass substrate due to difference in the thermal expansion coefficient between silicon and glass [11]. Pulsed laser crystallization SiGe is therefore interesting in application to fabrication of TFT with a high carrier mobility. However, few researches have been reported on pulsed laser crystallization of Ge or SiGe films [12,13].

In this paper, we report fundamental properties of laser crystallization of Ge and SiGe films. Melt-regrowth dynamics of the films are discussed using transient conductance measurements. SiGe formation is also shown through intermixing of silicon and germanium in the case of Ge/Si layered structures. We also report grain boundary properties of poly-SiGe films with analysis using transmission electron microscopy (TEM) and optical reflectivity measurements.

2. Experiments

Pulsed laser induced melting followed by regrowth was investigated using the transient conductance method [14]. Amorphous Ge (a-Ge), a-Ge/a-Si, SiGe alloy and a-Si films were formed on quartz substrate at room temperature by methods of plasma sputtering and molecular-beam deposition in a high vacuum [13]. The aluminum-gap electrodes with a width and length of 0.14 and 0.2 cm were then formed by thermal evaporation. Islands of Ge, Ge/Si and Si films were also defined. Electrical voltages were applied to the electrodes. Pulsed-308-nm-XeCl excimer laser with a pulse width of 30 ns at the half intensity was irradiated to samples from the rear side through the quartz substrate in order to heat the sample uniformly by avoiding a reduction of laser intensity caused by the optical interference at the edges of the Al electrodes. Significant heat diffusion into the substrate resulted in that the sample top surface is heated to

* Corresponding author.
  E-mail address: tsamesim@cc.tuat.ac.jp (T. Sameshima).

the highest temperature. The transient change in the voltage at the 50-Ω-load resistance connected between an electrode of samples and ground was measured by a 1-GHz high-speed digital storage oscilloscope during and after pulsed-XeCl excimer laser irradiation. A change in the conductance of the films caused by laser irradiation was estimated from the change in the voltage at the load resistance.

For structural analyses of the Ge, SiGe and Si films, we conducted laser crystallization of SiGe alloy films and measurements of Raman scattering spectra using 532 nm excitation laser, optical reflectively spectra as a function of wavelength from 250 to 750 nm and transmission electron microscopy (TEM).

3. Results and discussion

Fig. 1 shows the transient conductance per unit area from laser irradiation for 70-nm-thick Ge films (Fig. 1a) and 50-nm-thick Si films (Fig. 1b) with different laser energy densities. High electrical conductance of the germanium appears at 100 mJ/cm^2 because of laser induced melting. The electrical conductance rapidly increased 10 ns after
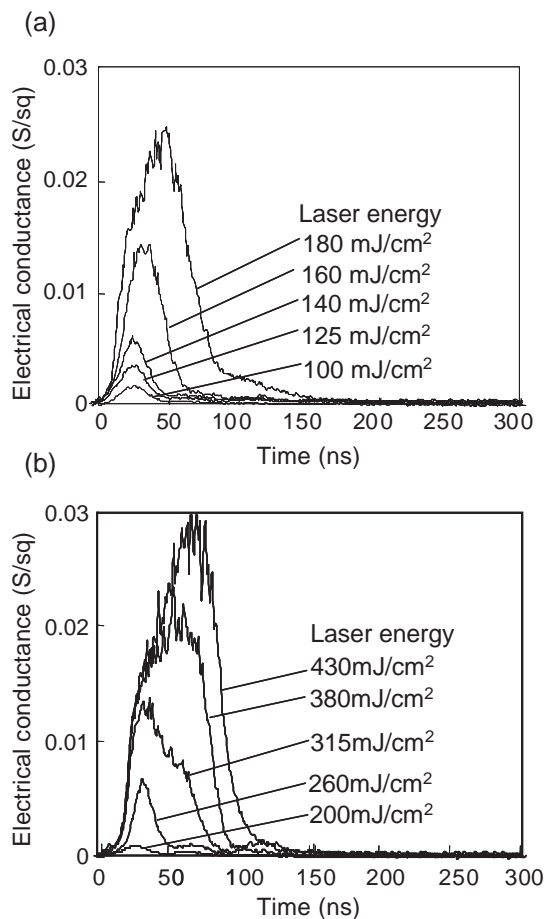

Fig. 1. Transient conductance per unit area with time for 70-nm-thick Ge films (a) and 50-nm-thick Si films (b). 308-nm-pulsed-XeCl excimer laser with 30-ns FWHM was irradiated at 0 ns at room temperature.

laser irradiation. After the peak maximum, it rapidly reduced coincidentally with decreasing laser intensity. The maximum electrical conductance increased as the laser energy increased. It means that the Ge films were rapidly melted into deep region by laser heating with high intensity. On the other hand, a high laser energy above 200 mJ/cm^2 was necessary to observe a significant increase in the electrical conductivity for Si as shown Fig. 1b. This is because of the high melting point of silicon films. The electrical conductance increased 20 ns after laser irradiation. It took some time to heat silicon to the melting point. The maximum electrical conductance monotonously increased as the laser energy increased. Very rapid solidification was observed at 430 mJ/cm^2. High energy laser irradiation induced complete melting silicon films in the whole thickness. Molten silicon films kept in the liquid state and the latent heat was not released when it cooled below the melting temperature (undercooling). The undercooled liquid silicon rapidly solidified and the latent heat was released simultaneously from the whole thickness [15].

Fig. 2a shows the maximum electrical conductance per unit area as a function of the laser energy. The threshold energy of increase in the electrical conductance indicates the melting threshold of the films. The ratio of the threshold energy for Ge and Si films was 0.55 (=110/200). It was understood well by reflectivity loss $(1-R)$ at 308 nm and the melting temperature T_m measured from room temperature; $[T_m^{Ge}/(1-R^{Ge})]/[T_m^{Si}/(1-R^{Si})]=[920/0.55]/[1400/0.52]=0.62$. The increasing rate of the electrical conductance with laser energy indicates the increasing rate of melting depth with laser energy. It was naturally governed by the latent heat, which is 4171 J/cm^3 for Si and 2713 J/cm^3 for Ge. The conductance increasing rate for Ge was 0.31 S/J, which was 2.2 times higher than 0.14 S/J for Si. The Ge films are easily melted by laser irradiation with a small laser energy. Figs. 1 and 2a clearly show that the melting point and the latent heat govern the melting properties.

Fig. 2b shows the maximum conductance per unit area as a function of laser energy for layered structure of 12-nm-Ge/50-nm-Si/quartz. The maximum electrical conductance increased as the laser energy increased from 100 to 110 mJ/cm^2. This indicates that the Ge layer as melted by the laser irradiation. Decrease in the peak electrical conductance was observed at 130 mJ/cm^2, as shown in Fig. 2b. The maximum electrical conductance increased again as laser energy increased above 130 mJ/cm^2. Fig. 3 shows stokes Raman scattering spectra for the 12-nm-Ge/50-nm-Si/quartz layered structure with different laser energies. The transverse optical (TO) phonon peak of crystalline Ge appeared at laser energies from 100 to 110 mJ/cm^2. This shows that top Ge layer was independently crystallized. On the other hand, broadening of Ge–TO phonon peak and small TO phonon peak of Si–Ge bonding were observed for laser energies from 130 to 160 mJ/cm^2. SiGe complex crystalline was formed by the laser irradiation. Decrease in the electrical conductance shown in Fig. 2(b) occurred asso-
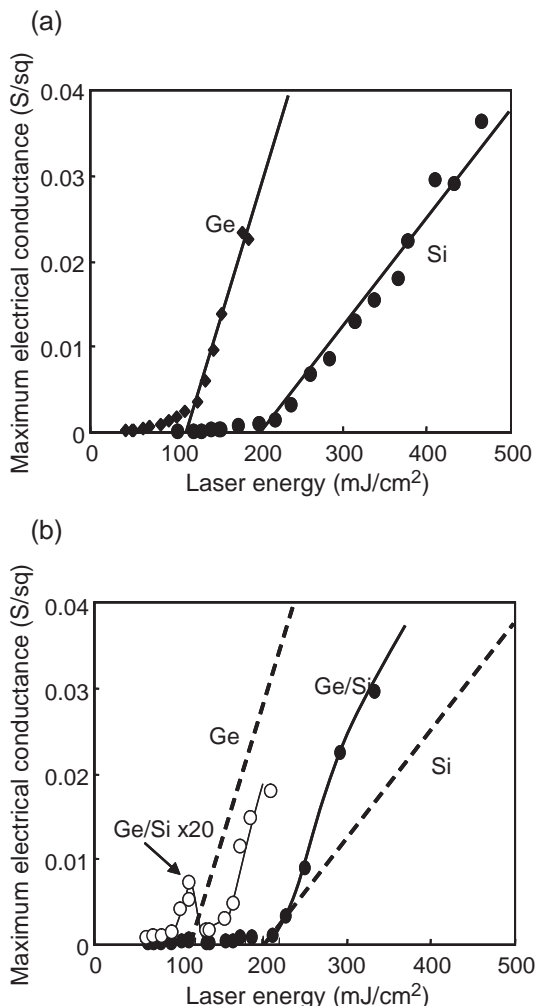
Fig. 2. The maximum electrical conductance per unit area as a function of laser energy for 70-nm-thick Ge and 50-nm-thick Si films formed on quartz substrates (a) and 12-nm-Ge/50-nm-Si formed on quartz substrate. Data 20 times magnified are also plotted in the low energy region. Dashed lines represent the maximum electrical conductance for Ge and Si films formed shown in (a).

Fig. 3. Stokes Raman scattering spectra for the 12-nm-Ge/50-nm-Si/quartz layered structure irradiated with different laser energies.

ciated with SiGe crystalline formation. Silicon atoms probably diffused into Ge films from the underlying silicon film during melting of the Ge layer. Diffusion of silicon atoms induced SiGe formation. Decrease in the electrical conductance resulted from the reduction of molten region due to SiGe formation with a high melting point compared with pure germanium. No silicon peak was observed in Raman spectra for laser energy up to 160 mJ/cm^2, which was lower than the melting threshold of silicon films. The Ge layer was changed to SiGe in the energy range between 130 and 160 mJ/cm^2. Significant increase of the peak electrical conductance was observed for laser energy above 200 mJ/cm^2. This results from the silicon layer melted by laser heating. The increasing ratio of the electrical conductance was high and close to that of pure Ge case for low energy condition near 200 mJ/cm^2. On the other hand, it was low close to that of pure Si for high energy conditions, as shown in Fig. 2(b). Si layer melting probably induced
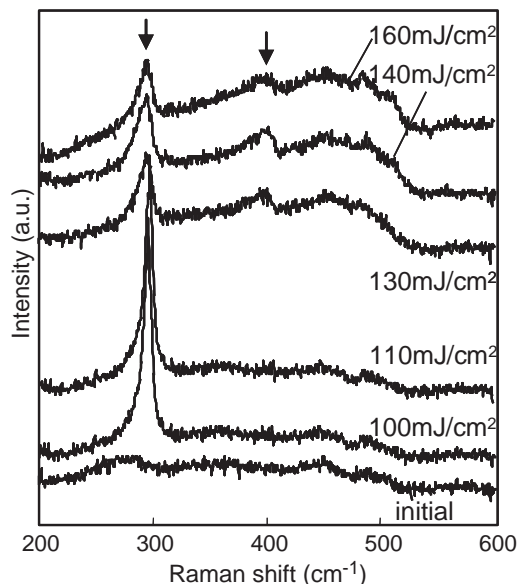
significant inter-diffusion of Ge and Si atoms from the top and bottom layers. SiGe formation proceeded in the molten region and reduced the latent heat for melting compared with that for melting of pure silicon. Because the molten thickness of the Si layer was thin for a laser energy near 200 mJ/cm^2, Ge concentration kept high in the top SiGe. Irradiation with high laser energy melts silicon in deep region. Ge atoms in 12-nm-Ge deeply diffused into silicon layer so that a SiGe layer with low Ge concentration was probably formed.

50-nm-thick-a-SiGe alloy films were crystallized in order to investigate grain boundary properties. Fig. 4 shows bright-field images of TEM for poly-$Si_{0.4}Ge_{0.6}$ films crystallized at 360 mJ/cm^2. The films were crystallized well and crystalline grains were close to each other. The size of crystalline grains increased as the germanium concentration
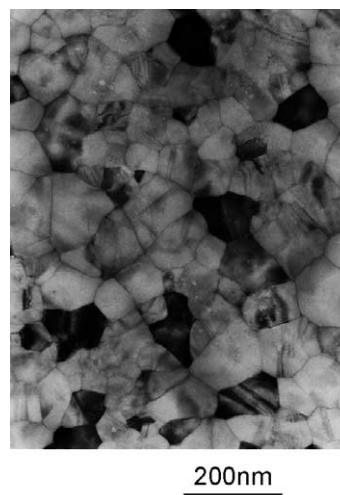

200nm

Fig. 4. Bright-field images of TEM for poly-$Si_{0.4}Ge_{0.6}$ films crystallized at 360 mJ/cm^2.
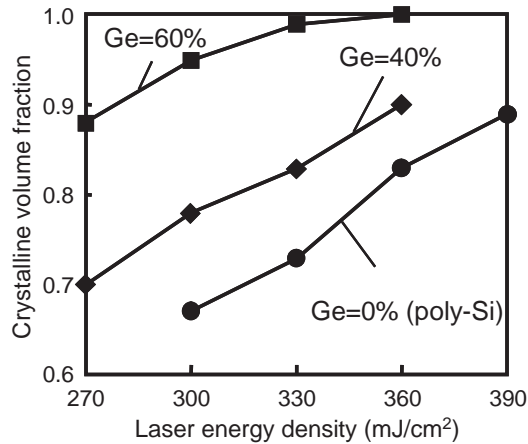
Fig. 5. The crystalline volume ratio of poly-SiGe films as a function of the laser energy density for different Ge concentrations.

increased. The average grain size was 120 nm, while it was 60 nm for pure silicon films. From the transient conductance measurement, $Si_{0.4}Ge_{0.6}$ films were melted deep and solidified rapidly. Deep melting and rapid solidification induced formation of large crystalline grains. The crystalline volume ratio was estimated by analysis of E_2 peak, which appeared around 275 nm in optical reflectivity spectra, using a numerical calculation program constructed with Fresnel coefficient method. The effective complex refractive index n_p of the poly-SiGe films is given by

$$n_p = Cn_c + (1 - C)n_a,$$

where C is crystalline volume ratio, n_c and n_a are the complex refractive indexes of single-crystalline and amorphous SiGe [16–19]. The best fitting of the calculated reflectivity spectra to experimental ones gave the crystalline volume ratio.

Fig. 5 shows the crystalline volume ratio of poly-SiGe and poly-Si films as a function of the laser energy density for different Ge concentrations. The crystalline volume ratio increased as the laser energy density increased. Moreover, the crystalline volume ratio increased as Ge concentration increased. In the case of poly-Si films, the crystalline volume ratio was 0.85 at a laser energy density of 360 mJ/cm². This means that only 85% region had the electrical-band structure of crystalline silicon and the residual 15% region had a band structure associated with disordered bonding states. The crystalline volume ratio increased to 1.0 as the Ge concentration increased to 60% within the resolution of the analysis of ~0.03 at 360 mJ/cm². An important reason of the high crystalline volume ratio close to 1.0 was the increase in the grain size. The formation of large grains resulted in a small area of peripheral grain boundaries per unit area. We measured the total length of grain boundaries per unit area, L, which was estimated from the TEM photographs. 1−(Crystalline volume ratio) gave the electrical disordered area. The effective width of electrical disordered states at grain boundaries was estimated by [1−(Crystalline vol-

ume ratio)]/L. $Si_{0.4}Ge_{0.6}$ films had a width of disordered states was 1.9 nm at most, while the effective width was about 5 nm for pure Si films. Ten lattice layers had electrical disordered states at grain boundaries. It is interesting that laser crystallized SiGe films with a high Ge concentration of 60% had a narrow width of grain boundaries and a large grain size. Disordered electronic states were reduced by Ge incorporation.

4. Summary

We reported crystalline formation of Ge and SiGe alloy films formed on quartz glass substrates using 308-nm-pulsed-XeCl excimer laser irradiation. Amorphous films were initially formed. The dynamics of melting followed by solidification of the films were investigated using transient conductance measurement. Germanium films were rapidly melted and solidified because of low latent heat compared with silicon films. It resulted in high crystallization velocity. 12-nm-Ge/50-nm-Si layered samples were also irradiated with laser. A decrease of the maximum electrical conductance was observed for irradiation at 130 mJ/cm². Raman scattering measurements indicated the formation of a silicon–germanium alloy through diffusion of Si atoms into the Ge liquid layer. For irradiation by higher laser energy, increasing ratio of maximum electrical conductance was higher than that of pure silicon case because SiGe formation occurred in silicon layer and the latent heat energy decreased. The crystalline volume ratio was estimated almost 1.0 for $Si_{0.4}Ge_{0.6}$ films because of small disordered electronic states. The effective width of grain boundary was estimated as 1.9 nm using analyses of optical reflectivity and grain size.

References

[1] M. Miyao, K. Nakagawa, Jpn. J. Appl. Phys. 33 (1994) 3791.
[2] F.M. Bufler, B. Meinerzhagen, J. Appl. Phys. 84 (1998) 5597.
[3] N. Sugii, K. Nakagawa, S. Yamaguchi, M. Miyao, Appl. Phys. Lett. 75 (1999) 2948.
[4] T. Sameshima, S. Usui, M. Sekiya, IEEE Electron Device Lett. EDL-7 (1986) 276.
[5] K. Sera, F. Okumura, H. Uchida, S. Itoh, S. Kaneko, K. Hotta, IEEE Trans. Electron Devices 36 (1989) 2868.
[6] H. Kuriyama, T. Kuwahara, S. Ishida, T. Nohda, K. Sano, H. Iwata, S. Noguchi, S. Kiyama, S. Tsuda, S. Nakano, M. Osumi, Y. Kuwano, Jpn. J. Appl. Phys. 31 (1992) 4550.
[7] E.L. Mathé, J.G. Maillou, A. Naudon, E. Fogarassy, M. Elliq, S. De Unamuro, Appl. Surf. Sci. 43 (1989) 142.
[8] A. Kohno, T. Sameshima, N. Sano, M. Sekiya, M. Hara, IEEE Trans. Electron Devices ED-42 (1995) 251.
[9] S. Uchikoga, N. Ibaraki, Thin Solid Films 383 (2001) 19.
[10] H. Watakabe, T. Sameshima, IEEE Trans. Electron Devices 49 (2002) 2217.
[11] S. Higashi, N. Andoh, K. Kamisako, T. Sameshima, Jpn. J. Appl. Phys. 40 (2001) 731.

[12] T. Sameshima, S. Usui, Proc. Mat. Res. Soc. Symp. 258 (1992) 117.

[13] H. Watakabe, T. Sameshima, H. Kanno, T. Sadoh, M. Miyao, J. Appl. Phys. 95 (2004) 6457.

[14] T. Sameshima, M. Hara, S. Usui, Jpn. J. Appl. Phys. 28 (1989) 1789.

[15] T. Sameshima, S. Usui, J. Appl. Phys. 74 (1993) 6592.

[16] C. Pickering, R.T. Carline, J. Appl. Phys. 75 (1994) 4642.

[17] J. Humlicek, M. Garriga, M.I. Alonso, M. Cardona, J. Appl. Phys. 65 (1989) 2827.

[18] R.T. Carline, C. Pickering, D.J. Robbins, W.Y. Leong, A.D. Pitt, A.G. Cullis, Appl. Phys. Lett. 64 (1994) 1114.

[19] S. Yamaguchi, N. Sugii, K. Nakagawa, M. Miyao, Jpn. J. Appl. Phys. 39 (2000) 2054.